Available online at www.sciencedirect.com
SCIENCE DIRECT®

Journal of the European Ceramic Society 24 (2004) 2485–2497

www.elsevier.com/locate/jeurceramsoc

# The effects of the PbO content upon the microstructure and the ferroelectric properties of undoped sol-gel derived PZT(53/47) fibers

R. Hansch[a,*], S. Seifert[a], W. Braue[b], D. Sporn[c], G. Müller[c]

[a]Forschungszentrum Jülich GmbH, 52425 Jülich, Germany
[b]German Aerospace Center (DLR), Materials Research Institute, 51147 Cologne, Germany
[c]Fraunhofer-Institut für Silicatforschung, Neunerplatz 2, 97082 Würzburg, Germany

Received 20 March 2003; received in revised form 12 July 2003; accepted 19 July 2003

**Abstract**

Sol-gel derived PZT(53/47) fibers with different PbO contents in the spinning sol were sintered with various buffers. Fiber stoichiometry, phase content and microstructure as well as the physical properties of the fibers were investigated. A fully densified microstructure was obtained for fibers 40 μm in diameter sintered as low as 900 °C via (1) an excess PbO content in the spinning sol of 6 mol% or higher and (2) a careful control of the sintering atmosphere by a $PbZrO_3/PbO$ buffer. Enhanced porosity was found only for fibers with lower PbO content in the spinning sol or for fibers sintered with $PbZrO_3/ZrO_2$ or $PbZrO_3$ buffer, respectively. The densification of PbO-deficient fiber batches is dominated by solid state sintering, while liquid phase sintering is promoted by excess PbO in the system. TEM investigations confirmed the homogeneous nature of the PZT fibers devoid of compositional gradients. Typical dielectric permittivities are in the range of 600–1000, the ferroelectric hysteresis loops are well pronounced with remanent polarization values of about 12 μC/cm$^2$ and coercivities between 1.2 and 1.4 V/μm. Strains of 0.10% were obtained.


*Keywords:* Electrical properties; PbO; Fibers; PZT; Sol-gel processes

## 1. Introduction

Multifunctional ceramic/polymer composites with integrated PZT fibers as the piezoactive constituent offer a high potential for sensoric and actoric applications.[1–5] Much effort has been directed towards the development of ultrasonic medical applications in the high frequency range as well as for the detection of forces, strains or vibrations.[5–8]

Most preparation routes for PZT fibers are different compared to the processing of conventional PZT mixed oxide materials.[9–12] In terms of their densification characteristics PZT fibers differ from PZT bulk ceramics of the same nominal composition due to their significantly increased surface to volume ratio. This fact plays an important role for the understanding of the effects of the processing parameters upon the development of the fiber microstructure.

As reported PZT fibers have been prepared from mixed-oxide powders, with fiber diameters in the range of 100 to 500 μm.[13–17] These rather thick fibers show very good piezoelectric properties with coupling coefficients $k_t$ of about 55%; however, some applications are limited due to the large diameters or limitations in fiber lengths. As an important advantage, these fibers provide easy handling similar to bulk ceramics prepared from mixed oxide powders.

In contrast, this research is focusing on thin sol-gel derived PZT fibers. The sol-gel process accounts for small fiber diameters down to 20 μm as well as for the preparation of batches of single fibers up to 0.5 m in length. Furthermore, sintering temperatures can be kept as low as 900 °C due to the fact, that the elemental distribution in the dried gel fiber is quite homogeneous. The high surface/volume ratio in PZT fibers requires a careful control of the PbO partial pressure during sintering. In order to compensate PbO losses and achieve a 100% PZT yield, two different experimental techniques were pursued:

* Corresponding author.
*E-mail address:* r.hansch@fz-juelich.de (R. Hansch).

0955-2219/$ - see front matter © 2003 Elsevier Ltd. All rights reserved.
doi:10.1016/j.jeurceramsoc.2003.07.008

1. The PbO level in the spinning sol was varied around the nominal stoichiometry of $(PbO)_{1.00+z}\cdot(Zr_{0.53}Ti_{0.47})O_2$ with $z=0.00$, thus covering PbO-deficient ($z=-0.06$) and PbO excess ($z=+0.14$) batch compositions.
2. A well-defined PbO partial pressure was established during sintering via different buffer systems.

The optimum sintering parameters for the PZT fibers will be identified through the combined effects of (1) buffer system variations, (2) variations of the PbO content in the spinning sol, and (3) of sintering experiments with different soaking times respectively. The microstructural development of PZT(53/47) fiber batches is derived via quantitative image analysis while the fiber nanostructure has been investigated through TEM studies. All batches are fully characterized in terms of di- and ferroelectric properties.

While this paper is directed towards optimization of sintering of undoped PZT(53/47) fibers, a companion paper[18] will discuss a similar approach for "soft" PZT fibers in the system PZT–SrKNb.[19]

## 2. Experimental

### 2.1. Preparation of sol-gel derived PZT(53/47)-fibers

PZT fibers were synthesized via a sol-gel process[20] with an oxidic bulk composition given by $(PbO)_{1+z}\cdot(Zr_{0.53}Ti_{0.47})O_2$ with $z=-0.06$, $+0.02$, $+0.06$ and $+0.14$ respectively. The resulting spinning mass has a solid content of 62–63 wt.%. The spinning mass was melted and extruded to fibers with diameters between 50 and 150 μm. The fibers were pyrolyzed in two steps (300, 600 °C) to prevent cracking during the removal of the organic ingredients.[7]

The pyrolyzed fibers were sintered at 900 °C in closed alumina crucibles. The heating rate was 1.25 K/min for all sintering experiments; the sintering time was 5 h, if not specified otherwise. The cooling rate was carried out with the furnace characteristics.

For controlling the PbO partial pressure during sintering, various PbO buffers were employed including (1) $PbZrO_3$(Chempur)/PbO(Alfa Aesar) (90/10 wt.%), (2) $PbZrO_3/ZrO_2$(Alfa Aesar) (92/8 wt.%) and (3) pure $PbZrO_3$. The latter was used as a standard puffer system. For comparison, sintering experiments devoid of a buffer system were also conducted.

### 2.2. Composite preparation

For the ferroelectric characterization 1–3-composites with fiber contents of 20–30 vol.% were prepared by aligning fibers parallel and infiltrating them with an epoxy resin. The fiber composites were diced perpendicular to the fiber orientation into thin discs, ground and polished down to a thickness of about 500 μm. For the microstructural and ferroelectric characterization gold electrodes were sputtered onto the surfaces of the samples (SCD 040, Balzer).

### 2.3. Microstructural characterization of the fibers

The chemical composition of the fibers was characterized by microprobe analysis (CAMECA SX 50). Phase analysis of the sintered fibers was conducted with powder X-ray diffractometry (Philips 1710). Scanning electron microscopy (SEM) (Hitachi S-800) was carried out on fibers and 1–3 composites. The residual porosity and the grain size distribution of the fibers were derived from polished and chemical etched composite surfaces via quantitative image analysis.

A Philips Tecnai F 30 transmission electron microscope operating at 300 kV acceleration voltage was employed for analysis of the nanoscale microstructure of PZT fibers. The preparation of TEM cross-section specimens[21] of PZT fibers via argon-ion beam thinning was severely impaired due to the non-uniform thinning behavior of the perowskite phase(s), percolation of nanopores and local amorphization of PZT due to radiation damage accumulated during argon ion beam bombardment. The problem was bypassed by utilizing crushed PZT fiber grain suspensions instead which worked sufficiently for conventional electron microscopy and small probe microanalysis.

### 2.4. Mechanical testing

The tensile strengths of PZT-monofilaments were tested in a uniaxial tensile testing apparatus (Zwick, Germany) with a constant crosshead speed of 1.5 mm/min. The sample preparation and the measurements were conducted according to the European prestandard for tensile strength determination of ceramic filaments.[22]

### 2.5. Ferroelectric and electromechanical testing

Poling of the composites was performed with 5 kV/mm at 80 °C for 2 h and cooling down in the electric field. Dielectric permittivities $\epsilon_r$ and $\epsilon_{33}$ were evaluated before and after poling, respectively, the dielectric loss tan δ was measured after poling. Ferroelectric measurements were carried out with a simple current–voltage converter, the strain–voltage dependence was measured[1] with an apparatus described elsewhere.[23]

[1] By the courtesy of R. Steinhausen, Martin-Luther-University, Halle, Germany.

## 3. Results and discussion

This paragraph is organized as follows: first, the effects of the PbO content in the spinning sol on the microstructure of the pyrolyzed fibers is discussed in Section 3.1. The complete characterisation of sintered PZT fibers with various lead contents in the spinning sol, sintered with a $PbZrO_3$ standard buffer system is described in Section 3.2, while Section 3.3 refers to the effects of various buffer systems on sintering of PZT fibers.

### *3.1. Pyrolyzed PZT(53/47) fibers: Microstructure and phase content*

Following a two-step pyrolysis for 12 h at 300 and 600 °C respectively, all pyrolyzed PZT-fibers show a typical core-shell structure (Fig. 1a). The grains in the outer region form a dense shell with grain sizes between 0.5 to 1 μm (arrows in Fig 1a), whereas the core region consists of fine-grained agglomerates with grains sizes between 100 and 150 nm and a high amount of porosity.

For excess-PbO pyrolyzed fibers little variations of the PbO, the $ZrO_2$, and the $TiO_2$ content across the fiber diameter were found via microprobe analysis (not shown here). These, however, were within the statistical data scattering of typically 2–3 wt.% and did not allow for a correlation between the compositional variations and the observed core–shell–mesostructure of the fibers.

In contrast, PbO-deficient pyrolyzed fibers showed a significant variation of the PbO content across the diameter (Fig. 1b). The PbO content decreased from 71 wt.% at the edge of the fiber to about 65 wt.% in the center, whereas the $ZrO_2$ and the $TiO_2$ contents increased from 19 to 22 wt.% and 11 to 13 wt.%, respectively, in the same direction. The compositional variations for PbO-deficient pyrolyzed fibers seem to be related to the larger fiber diameter of about 100–150 μm as compared to the lead-rich fibers with diameters of

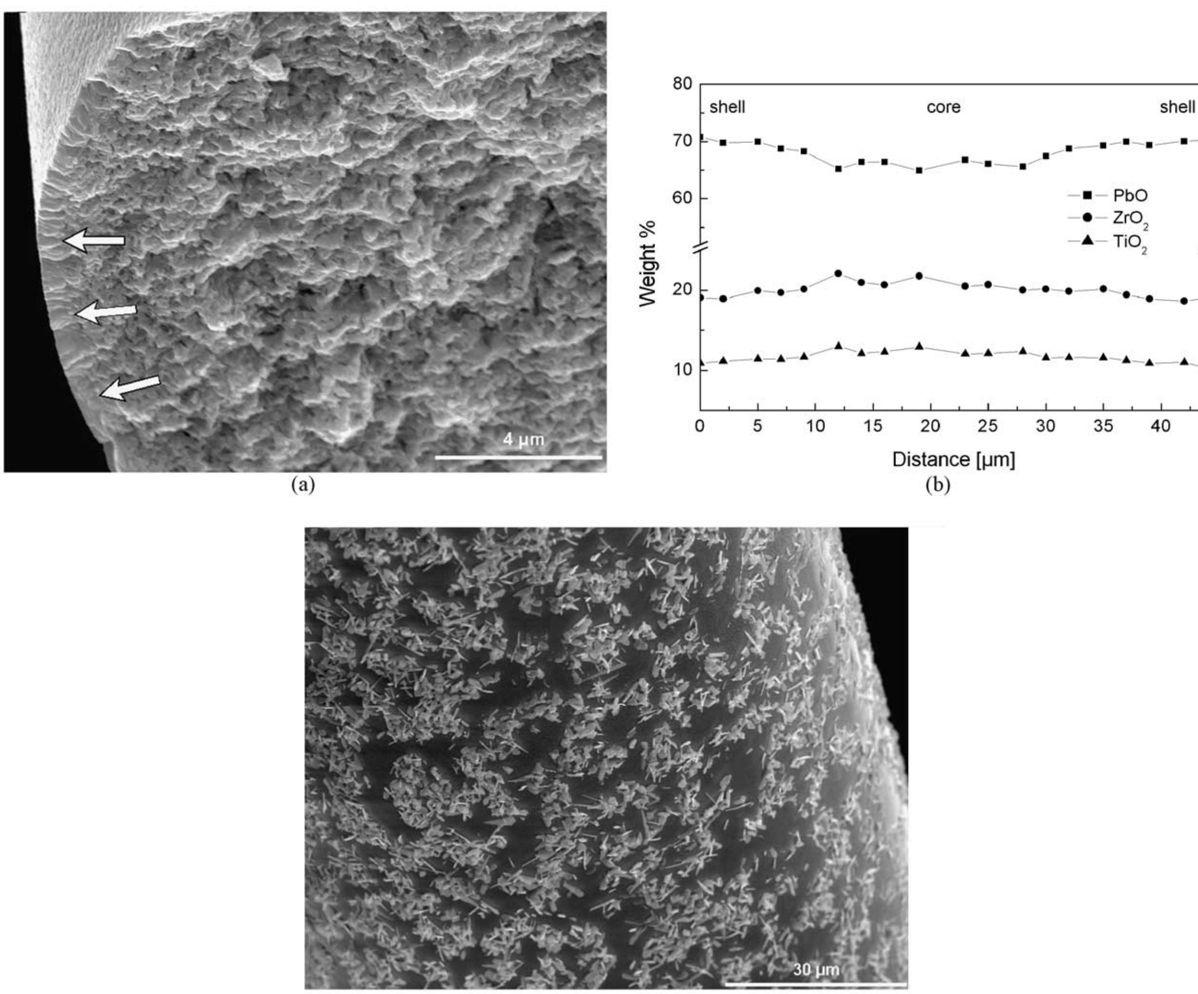


Fig. 1. (a–c) Microstructure of pyrolyzed PZT fiber with an understoichiometric PbO content of $z = -0.06$ in the spinning sol; (a) core/shell mesostructure, (b) compositional line scans across fiber cross-section via electron microprobe, (c) precipitation of small PbO crystallites on the fiber.

only 30–50 μm. For the PbO-deficient pyrolyzed batches reducing conditions during the first pyrolysis step (300 °C) can be supposed for the central fiber regions causing a reduction of PbO to metallic lead. The latter has a much higher vapour pressure and, as a consequence, can easily diffuse to the fiber periphery. During the second pyrolysis step (600 °C), this metallic lead can be reoxidized again. This reoxidation causes the formation of PbO microcrystallites at the fiber surface (Fig. 1c), as observed by SEM investigations. As a net effect an increase of the relative PbO content was detected close to the fiber surface of PbO-deficient fibers (Fig. 1b), which did not occur for the much thinner PbO-excess fibers.

Phase analysis via X-ray diffraction (Fig. 2) showed, that for excess-PbO pyrolyzed fibers no crystalline secondary phases (e.g. PbO), were observed within the detection limit. In contrast, PbO-deficient pyrolyzed fibers did reveal small amounts of PbO which is related to the aforementioned formation of PbO crystals at the fiber surface. Additional secondary phases, such as $ZrO_2$ or $PbTiO_3$, were not observed. (Fig. 2).

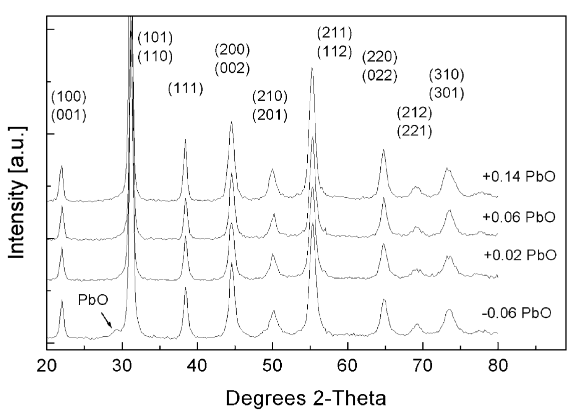


Fig. 2. XRD diffractograms of pyrolyzed PZT fibers at 600 °C with different PbO contents in the spinning sol. Only for PbO-deficient fibers has free PbO been detected as a secondary phase.

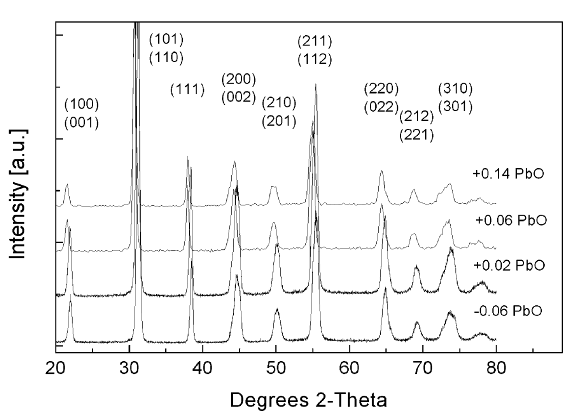


Fig. 3. XRD diffractograms of PZT fibers sintered at 900 °C with different PbO contents in the spinning sol. No secondary phases were found.

### 3.2. Sintered PZT fibers (I): PbO variations in the spinning sol

#### 3.2.1. Phase content of sintered PZT fibers

After sintering with a $PbZrO_3$ standard buffer system, all sintered fibers showed pure PZT in the XRD diffractograms, independently of the PbO-content in the spinning sol (Fig. 3). Within the detection limit of the diffractometer, no crystalline secondary phases such as $ZrO_2$, $PbTiO_3$, or PbO could be observed. Apparently the small amount of PbO detected on the surface of the PbO-deficient fibers after pyrolysis (see Section 3.1) had evaporated during sintering.

From the broad (200)/(002) and (310)/(301) peaks displayed in Fig. 3 the coexistence of the rhombohedral and tetragonal phase has been established for all sintered batches investigated.

The homogeneity of the batches and the lack of crystalline secondary phases even for the excess-PbO batch with $z = +0.14$ emphasize that the combined effects of (1) excess PbO in the spinning sol as well as (2) the partial pressure of PbO established in the crucible allow for complete transformation to PZT when employing the $PbZrO_3$ standard buffer system.

It should be noted that whenever an excess-PbO source is offered during sintering [either through the PbO content of the spinning sol and/or a PbO-rich buffer system exhibiting a higher PbO partial pressure than the $PbZrO_3$ standard buffer (see also Section 3.3)] an excess PbO-level of 2–3 mol% as compared to the nominal PZT composition is established in the sintered fibers as determined via ICP-AES analysis. As discussed in Section 3.2.3 a noncrystalline PbO-rich secondary phase has been identified for excess-PbO sintered batches via TEM.

#### 3.2.2. SEM investigations of sintered PZT fibers

As depicted in Figs. 4a,b, both, (1) PbO-deficient fibers as well as (2) batches exhibiting moderate excess-PbO levels up to $z = +0.02$, exhibit a similar gross microstructure consisting of a dense shell and a porous core. This core-shell mesostructure corresponds to that of the pyrolyzed fibers (Fig. 1a) indicating that for PbO-deficient batches or such fibers exhibiting a small excess-PbO level the pre-established microstructure cannot be overcome during sintering.

The porous core consists of idiomorphic grains of about 1 μm in size, the grains are connected by sintering necks. A bimodal grain size distribution with maxima between 1 and 3 μm was obtained from polished surfaces. The equiaxed grain morphology introduces a pillow-like fiber surface structure characterized by networks of 120° dihedral angles. Only little porosity could be found, intergranular defects such as cracks and pores have not been detected.

In contrast, excess-PbO PZT fibers with $z \geqslant +0.06$ did not reveal a correlation between the PbO content and the observed fiber microstructure. As shown in Fig. 4c,d, both samples achieved full densification. The grains exhibit a polyhedral shape with grain sizes up to 2 to 3 μm. Notches at grain boundaries and triple points were less pronounced as compared to PbO-deficient fibers. No core-shell effects as identified in PbO-deficient batches were observed, indicating, that the sintering mechanisms in the excess-PbO batches were strong enough to overcome the pre-established fiber-microstructure after pyrolysis and result in dense fibers with large grain sizes.

Both, fiber porosity and average grain sizes were determined as a function of the PbO content from polished fiber cross sections (Fig. 5). Porosity decreases with increasing PbO content in the spinning sol. The volume fraction of the porosity varies between 8 vol.% for PbO-deficient fibers and <1 vol.% for fibers with a

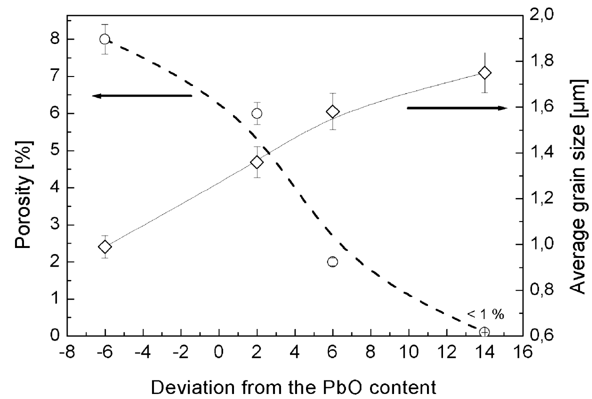


Fig. 5. The effect of excess PbO in the spinning sol on fiber porosity (left) and average grain size (right). As expected, grain sizes increase and porosity decreases with increasing PbO content in the spinning sol.

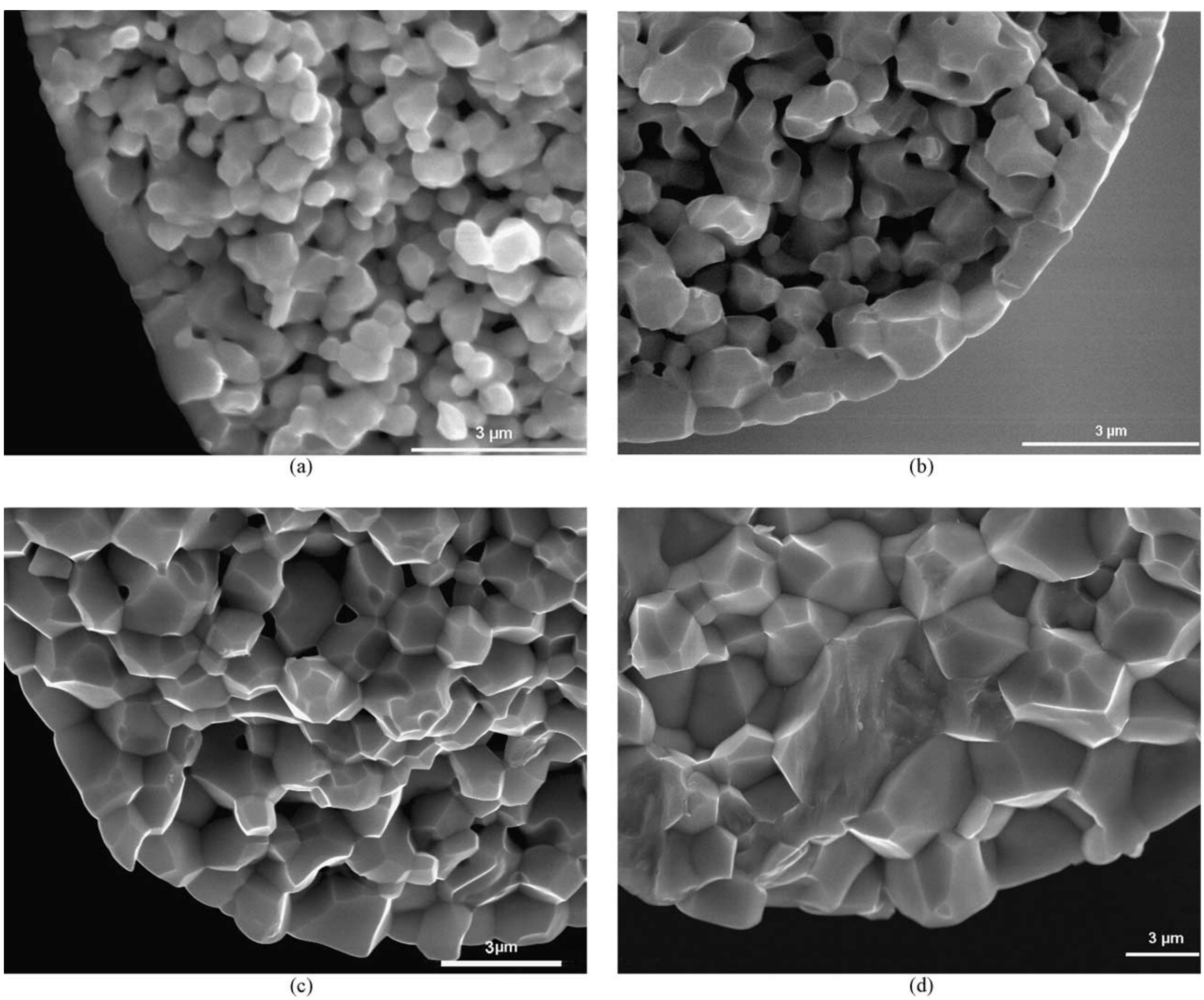


Fig. 4. Fracture surfaces of sintered PZT fibers; (a) PbO-deficient fibers (b) fibers with $z = +0.02$ excess PbO, (c) fibers with $z = +0.06$, (d) fibers with $z = +0.14$. Fibers with PbO deficiency and $z = +0.02$ excess PbO exhibit a composite mesostructure consisting of a dense shell and a porous core built of 1 μm sized PZT grains. In contrast fibers with an excess PbO content $z > +0.02$ were fully densified devoid of a core/shell mesostructure. Typical grain sizes are up to 2–3 μm.

PbO excess $z \geqslant = +0.06$. The average grain size scales with the PbO content of the spinning sol. For PbO-deficient fibers an average grain size of about 1 μm was found within a monomodal grain size distribution, whereas for PbO excess fibers average grain sizes between 1.4 and 1.8 μm were found.

As expected, fiber fracture surface structures vary significantly with the PbO content of the spinning sol. PbO-deficient fibers are characterized consistently by an intercrystalline fracture mode, while PbO excess fibers show a mixed mode behavior with transcrystalline fractures of up to 50%. Most transcrystalline fractures were found for fibers with large grain sizes as well as in the outer region of the fibers.

#### 3.2.3. TEM investigations of sintered PZT fibers with varied PbO content in the spinning sol

The TEM results corroborated the general microstructural features of sintered PZT fibers as derived from XRD and SEM investigations. The fiber microstructure is free of pores and homogenous two-phase ($F_t$, $F_r$) perowskite.

Z-contrast imaging with a high-angle annular dark field (HAADF) detector as well as EDS line scans across individual PZT grains performed in STEM mode did not reveal compositional gradients. Typically, PbO-deficient batches were devoid of non-PZT secondary phases at grain boundaries and triple grain junctions (Fig. 6).

Excess-PbO batches exhibited an intergranular non-crystalline PbO-rich secondary phase (Fig. 7a). Small probe microanalysis from the non-crystalline phase (Fig. 7b) showed substantial Si and Pb concentrations

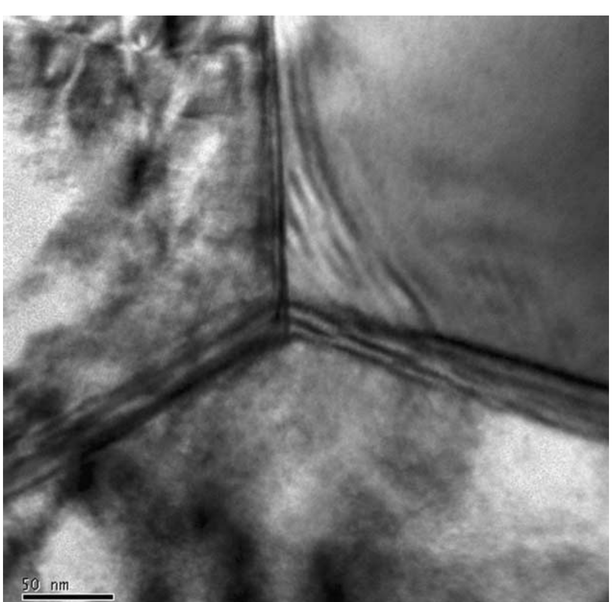


Fig. 6. Triple grain junction devoid of secondary phases from a sintered PbO-deficient PZT fiber (TEM, BF, 300 kV).

along with various amounts of Al, K, Ca, S, and Cl impurities. Through ICP analysis the origin of these impurities could be traced to intrinsic impurities of the precursors employed for spinning sol synthesis. In some cases HREM images obtained from amorphous regions did reveal nanocrystalline PbO particles embedded in the amorphous phase (Fig. 7c).

#### 3.2.4. SEM and TEM investigations of fibers with varied sintering times

Sintering experiments at 900 °C with varying holding times were performed for fiber batches as a function of the excess PbO content. Extending the holding times beyond 15 min for fiber batches with $z = +0.02$ did not result in a decrease in porosity. Their microstructure compares to that from fibers with only 5 min holding time at the same temperature. Grain growth did not set in before a holding time of 60 min. Sintering necks are abundant, however, the residual porosity is still of the order of 15%.

In contrast, for fiber batches with $z = +0.14$ the densification at 15 min holding time is almost complete with a residual porosity $<1\%$ (Fig. 8). Grains are faceted with grain sizes of approx. 1.5 μm, 120° dihedral angles are commonly observed in the grain boundary network.

The fast sintering kinetics of these PbO-excess PZT fibers along with the TEM evidence of a PbO-bearing, intergranular non-crystalline phase strongly suggests a liquid-phase sintering mechanism similar to observations from mixed oxide PZT systems.[9–12,24,25] According to Atkin and Fulrath[26] liquid phase formation will not occur below a threshold level of $z = +0.035$ PbO. This is in good agreement with our sintering experiments from PZT fibers, where excess-PbO batches with $z = +0.02$ batches still follow a solid state sintering process, while substantial liquid phase sintering was observed for $z = +0.06$ batches.

#### 3.2.5. Measurements of the tensile strength of sintered PZT fibers

The tensile strength of sintered PZT fibers was determined from stretched and coated fibers. Fiber stretching was realized by separating the fibers before sintering from each other; the coating was applied through a mixture of 7 vol.% polyvinylalkohole (PVA) and water. Compared to uncoated fibers with tensile strength of about 82 MPa, the fiber tensile strength was significantly enhanced by the PVA-coating to mean values of about 125 MPa. Nevertheless, the tensile strength data for both, the uncoated and the coated fibers, showed considerable data scatter up to 80%. This is primarily due to the sensitivity of the fibers against shear stress. For stretched and coated fibers a maximum tensile strength up to 149 MPa was measured; this value agrees well with the typical tensile strength level (75 MPa) reported for PZT bulk ceramics.[27]

### 3.2.6. Dielectric properties

For the calculation of the dielectric properties of the fibers, the capacitances of 1–3 composites containing the fibers, were measured: In Fig. 9 the $\epsilon_r$ values the unpoled fibers are depicted as a function of the PbO content of the spinning sol. Typical $\epsilon_r$ values for the fibers are between 600 and 1000; these values agree well with the data for bulk ceramics with comparable stoichiometry.[28,29] From Fig. 9 there might be a tendency of increasing $\epsilon_r$ with increasing PbO content, but the scattering of the data is too high for an unambiguous correlation. From SEM investigations it is known, that with increasing PbO content the porosity is decreasing; this should be accompanied by an increase in the dielectric permittivity. Nevertheless, with increasing PbO content the grain size is increasing drastically, too, and this should favour the opposite tendency, namely a decrease in the dielectric permittivity.

The substantial data scattering can be used as a quality indicator for both fibers and composites. The main reason for scattering may be due to fiber fractures during composite preparation caused by the nonoptimized fiber geometry. Also note that small fiber fractions only could be accomplished for those composites. Unfortunately, fiber fractures within the composite cannot be detected unambiguously; therefore, the reasons for the strong data scattering are not clear yet and requires further investigations.

From poled composites the permittivity was measured again. As can be seen from Table 1, $\epsilon_{33}$ after poling is

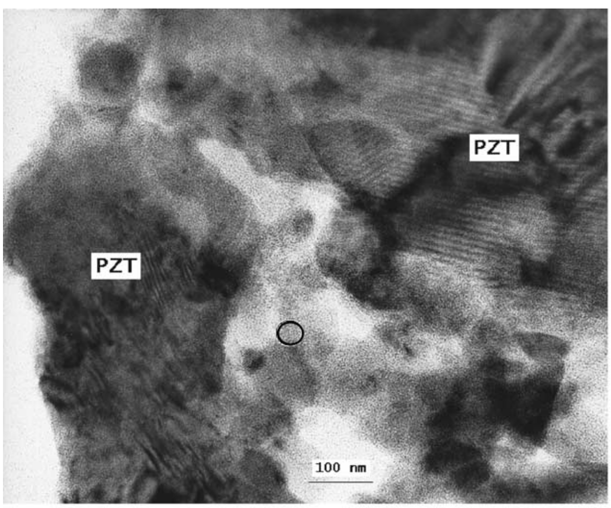


(a)

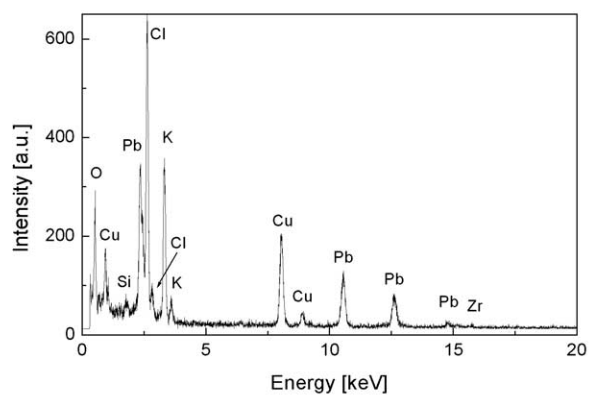


(b)

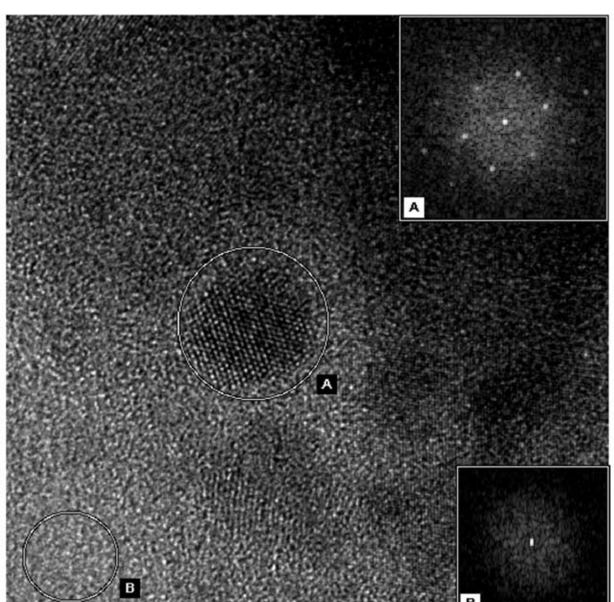


(c)

Fig. 7. Analytical TEM investigations from a multigrain junction in sintered PbO excess PZT fiber (crushed grain suspension); (a) low-magnification BF image; (b) EDS spectrum collected from the glassy phase with a X nm probe; (c) HREM image of PbO microcrystalls dispersed through the non-crystalline phase, displaying the encircled region in (a) at higher magnification.

lower compared to the initial value of the unpoled state. This effect can be attributed to a decrease in the domain wall contributions to the permittivity after poling.

#### 3.2.7. Ferroelectric and electromechanical properties

Hysteresis measurements were carried out at a frequency of 50 Hz. In Fig. 10 typical hysteresis loops with increasing applied field strength are shown. The characteristic ferroelectric properties from these measurements were summarized in Table 2. For all samples, good ferroelectric properties were obtained with a remanent polarization of about 10 $\mu C/cm^2$ and a coercivity of about 1.2–1.3 V/μm. Again, no unambiguous correlation could be established between the ferroelectric properties and the PbO content of the spinning sol, i.e. the microstructure of the fibers. This may be again due to the counteracting effects of increasing grain sizes and decreasing porosities with increasing PbO content.

Electromechanical hysteresis loops were obtained from selected composites, too. As can be seen from Fig. 11, typical strains of up to 0.10% could easily be obtained with voltages of 6 V/μm, i.e. about three times of $E_c$. The coercivities from the strain–voltage measurements correspond well with those of the ferroelectric ones, as a tendency the latter seem to be somewhat higher.

### 3.3. Sintered PZT fibers (II): variations of the buffer system

In order to address the effect of different PbO partial pressures in the sintering atmosphere, 90:10 $PbZrO_3$:PbO, 92:8 $PbZrO_3$:$ZrO_2$, and pure $PbZrO_3$

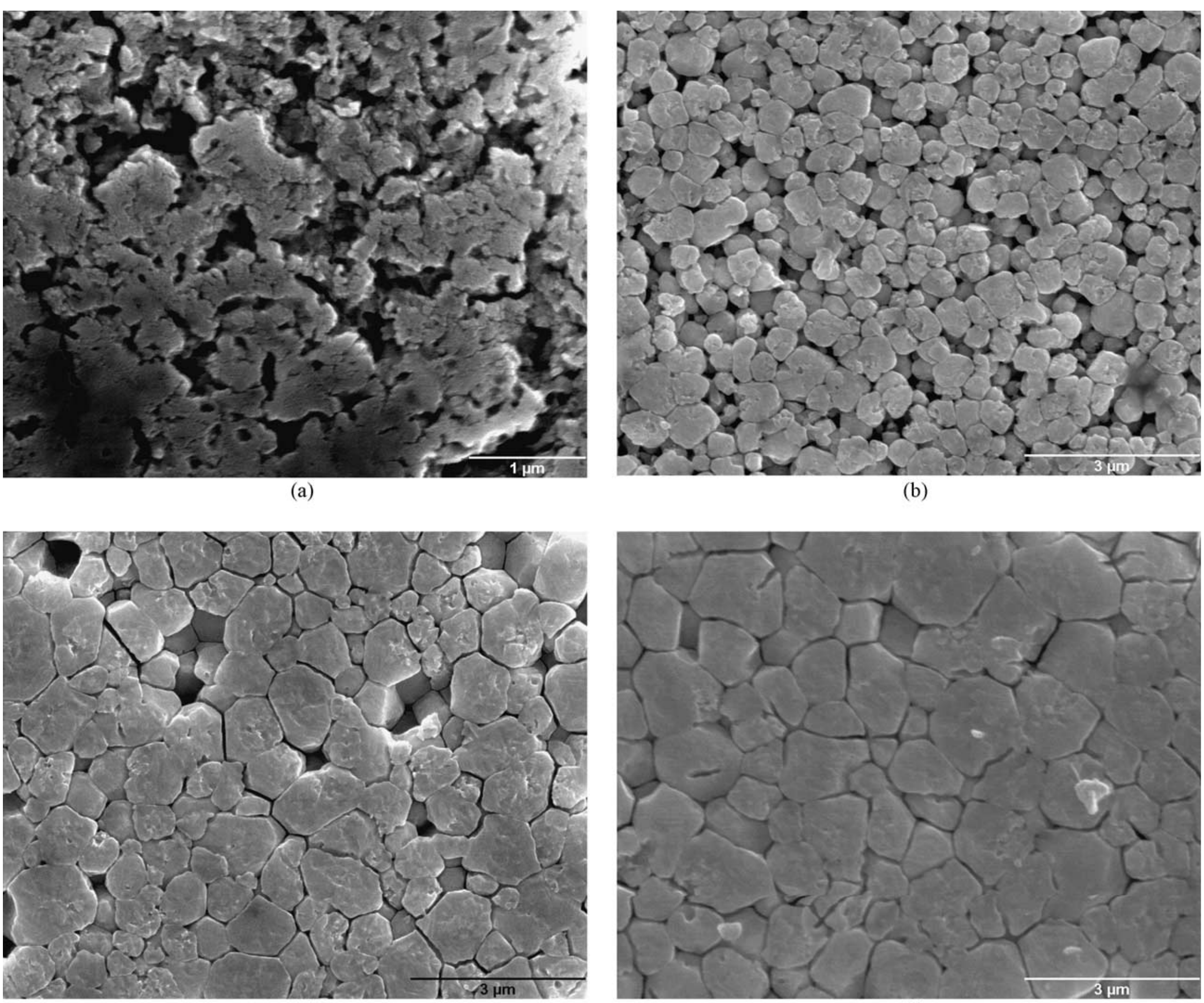


Fig. 8. Polished and etched surfaces of $z=+0.14$ excess PbO PZT fibers sintered at 900 °C with a $PbZrO_3$ buffer. The microstructural development is displayed at sintering times of (a) 5 min; (b) 10 min; (c) 15 min; (d) 60 min (note different scale).

buffers were employed for sintering of both, PbO-deficient and PbO-excess fiber batches and compared to the "no buffer" sintering experiments.

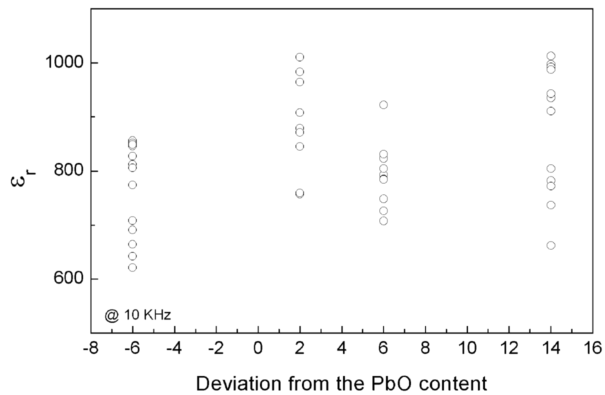


Fig. 9. Dielectric permittivity $\epsilon_r$ of unpoled PZT(53/47) fibers as a function of the PbO content of the spinning sol.

Table 1
Permittivities of PZT fibers with different PbO contents in the spinning sol

| | PbO content in the spinning sol $z$ | | | |
|---|---|---|---|---|
| | −0.06 | +0.02 | +0.06 | +0.14 |
| $\epsilon_r$ | 770±90 | 740±180 | 720±130 | 880±120 |

### 3.3.1. Microstructural assessment of PZT fibers sintered with different buffers systems

All sintered excess-PbO batches are devoid of crystalline secondary phases, irrespectively of the buffer system employed. The fibers consist of homogenous PZT defined by a Zr/Ti-ratio close to the morphotropic phase transition (not shown here). For the PbO-deficient batch ($z$ = −0.06) the sintering experiments yield homogeneous PZT for all buffer systems, too. No crystalline secondary phases such as unreacted $ZrO_2$ or $PbTiO_3$, or excess PbO from the buffer systems used could be identified within the XRD detection limit. The relatively broad (200)/(002)- and (310)/(301)-peaks suggest the coexistence of both, the rhombohedral and the tetragonal perowskite phase (Fig. 12) in the sintered PbO-deficient batch.

In contrast, PbO-deficient fibers sintered without any buffer system did not convert to homogeneous PZT, containing unreacted $ZrO_2$ as an additional phase. As a consequence, the $ZrO_2$ level of the PZT crystals is shifted towards lower $ZrO_2$ concentrations compared to the initial $ZrO_2$ content thus reducing the amount of the rhombohedral phase. This causes a relative increase of the tetragonal, $PbTiO_3$-rich phase, which is expressed in the clear splitting of (200)/(002)-, (210)/(201)-, and (310)/(301)-interferences in the corresponding diffractograms (Fig. 12).

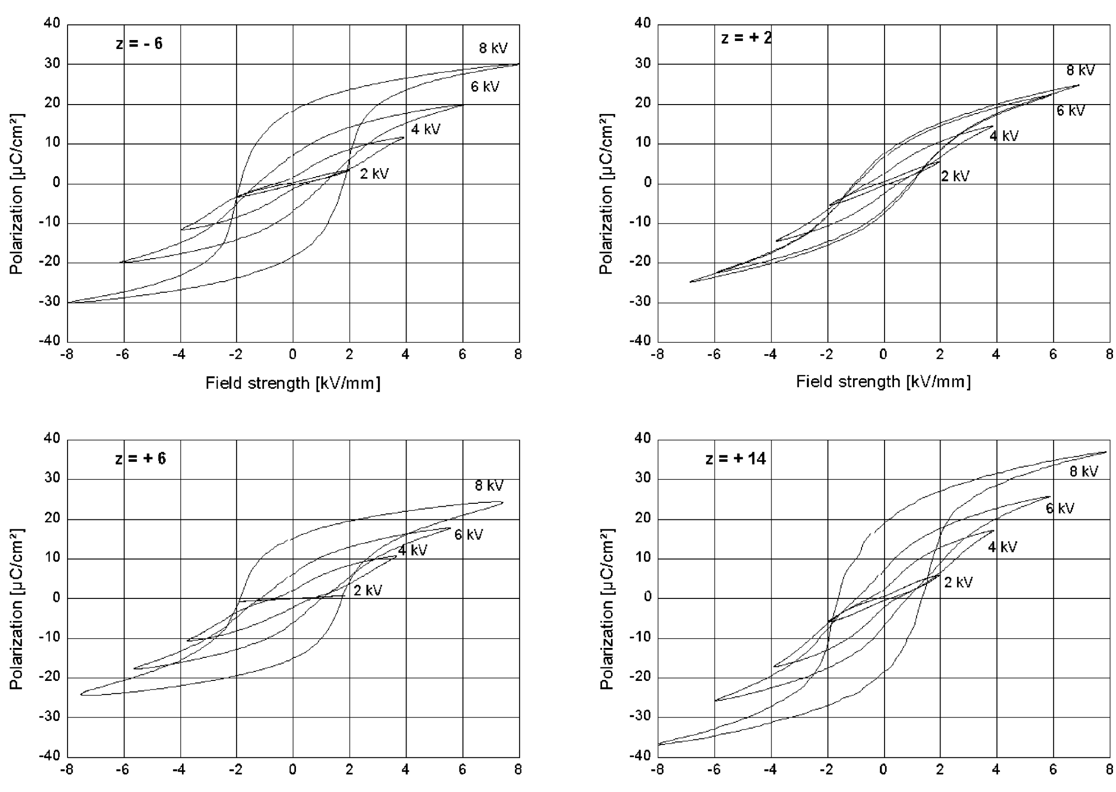


Fig. 10. Ferroelectric hysteresis loops of sintered PZT fibers with different PbO contents in the spinning sol: The measurements were carried out for different applied field strengths after 1000 cycles; PbO content of the fibers: (a) $z$ = −0.06; (b) $z$ = +0.02; (c) $z$ = +0.06; (d) $z$ = +0.14.

Table 2
Characteristic ferroelectric properties of PZT fibers with different PbO contents in the spinning sol

| | PbO content in the spinning sol $z$ | | | |
|---|---|---|---|---|
| | −0.06 | +0.02 | +0.06 | +0.14 |
| Coercivity $E_c$ [V/μm] | 1.4±0.1 | 1.2±0.2 | 1.6±0.2 | 1.3±0.2 |
| Max. polarization $P_{max}$ [μC/cm$^2$] | 24±2 | 21±2 | 24±2 | 28±2 |
| rem. Polarization $P_{rem}$ [μC/cm$^2$] | 11±1 | 8±1 | 14±1 | 12±1 |

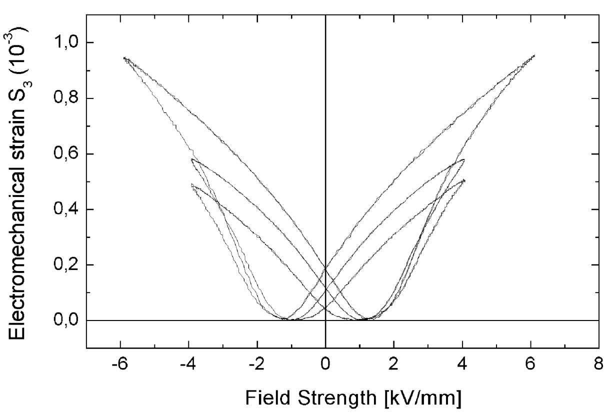


Fig. 11. Typical electromechanical hysteresis loops for PZT fibers in a 1–3 composite. The fibers have a PbO excess of $z = +0.06$ in the spinning sol.

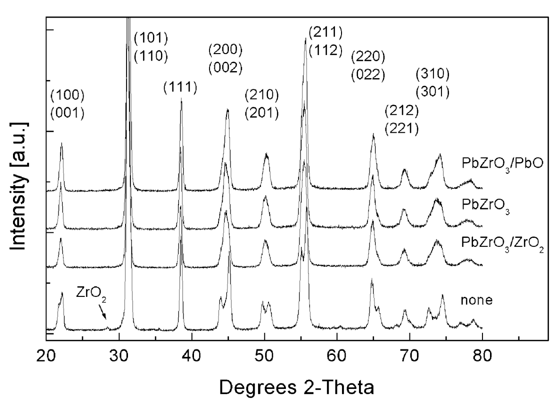


Fig. 12. XRD diffraction patterns for PbO-deficient PZT fibers sintered with various buffer systems and without any buffer (see arrow). For all batches sintered with buffers, no secondary phases were observed. In contrast, the fibers sintered without any buffer showed $ZrO_2$ as a secondary phase.

These observations indicate that a small amount of excess PbO in the initial batch composition may indeed be sufficient to yield a 100% PZT without the need of an additional buffer system. However, it is important to note that complete transformation to perowskite phase does not necessarily account for full densification of the fibers microstructrure. Thus, it is mandatory for optimization of PZT sintering parameters to consider the effects of buffer systems.

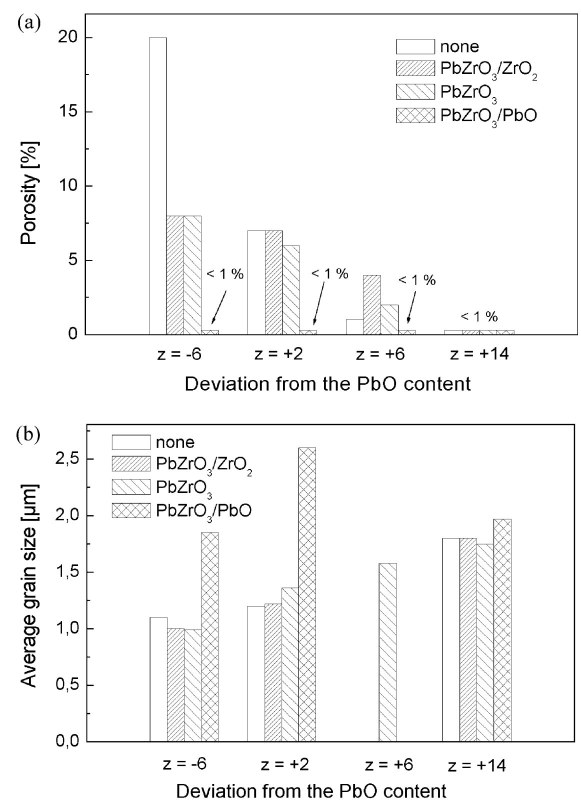


Fig. 13. Porosity (a) and average grain size (b) of PZT fibers with various PbO contents in the spinning sol sintered at 900 °C for 5 h with different buffers system and without a buffer.

The essence of the sintering experiments presented in this study is summarized in Fig. 13a and b, demonstrating the effects of different buffer systems upon the residual fiber porosity and grain sizes as a function of the PbO-levels in the spinning sol. The fiber porosity and the composition of the buffer systems employed are clearly correlated.

Independently of the amount of PbO in the spinning sol, fibers sintered without a buffer system show the highest porosity. PbO-deficient fibers sintered with no buffer system exhibit a porosity of 20 vol.%, which decreased to 8 vol.% when utilizing a $PbZrO_3/ZrO_2$ or a $PbZrO_3$ buffer system instead. A residual porosity of less than 1 vol.% could be achieved with a $PbZrO_3/PbO$ buffer.

For batches exhibiting small excess-PbO levels, the influence of the buffer systems is comparable, although

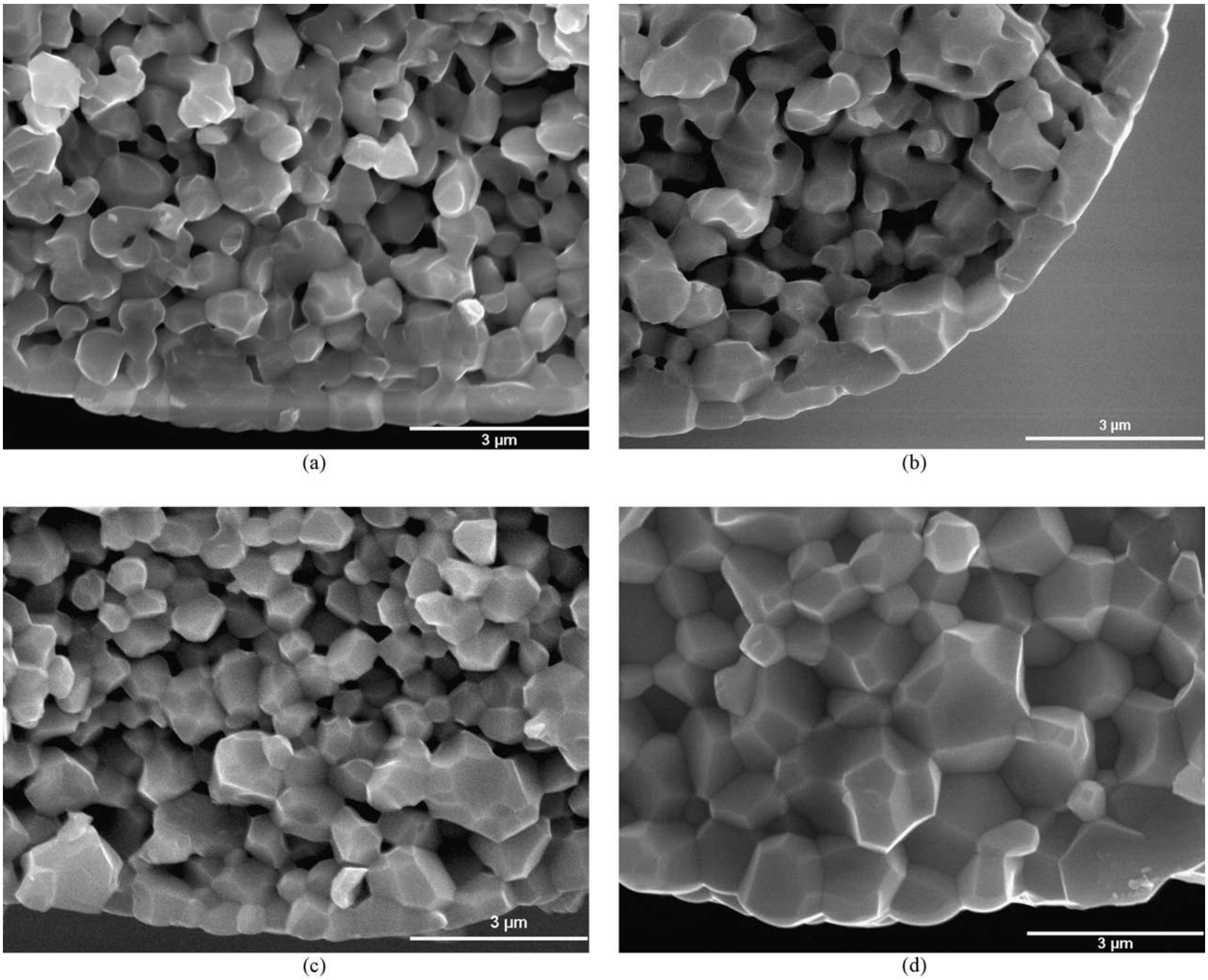


Fig. 14. Fracture surfaces of PZT fibers with a PbO excess of $z=+0.02$ in the spinning sol by using different buffers during sintering at 900 °C for 5 h; devoid of a buffer system (a), with $PbZrO_3/ZrO_2$ (b), $PbZrO_3$ (c) and $PbZrO_3/PbO$ (d).

Table 3
Dielectric permittivities of two PZT fiber batches with different PbO content in the spinning sol sintered with various buffer systems

| | PbO content in the spinning sol | |
|---|---|---|
| | $z=+0.02$ | $z=+0.14$ |
| Without additional buffer | 430±60 | 720±120 |
| $PbZrO_3/ZrO_2$ buffer | 810±120 | 1020±150 |
| $PbZrO_3$ buffer | 810±140 | 970±40 |
| $PbZrO_3/PbO$ buffer | 730±70 | 1420±230 |

somewhat less pronounced than in the case of PbO-deficient batches. The data indicate a decreasing beneficial effect of the buffer system with increasing PbO content in the spinning sol. As a consequence, for high excess PbO contents in the spinning sol, the PbO excess will compensate for a lack of buffer system during sintering and still achieve full densification.

Increased average grain sizes are obtained when using a higher PbO content in the spinning sol (Fig. 13b). Fibers with $z=+0.02$, $+0.06$, and $+0.14$, yield grain sizes of 1.5, 1.7 and 1.8 µm, respectively. Again, the influence of the buffer system on the grain size decreases with increasing amount of PbO in the spinning sol.

Rather similar fiber microstructures result from sintering experiments with the both buffer systems consisting of $PbZrO_3$ only and $PbZrO_3/ZrO_2$, as shown in Fig. 14 for the fiber batches with $z=+0.02$. The strong increase of the grain size when using the $PbZrO_3$/PbO-buffer suggests, that the PbO excess level in these batches is too low to compensate for PbO losses under the constraints of all PbO-deficient buffer systems employed.

For the $PbZrO_3$/PbO-buffer experiment grain growth has set in for all fiber batches, indicating that the soaking time can be substantially reduced in order to achieve small grain sizes. As discussed in Section 3.2.5, the sintering kinetics in PbO-saturated systems are fast accounting for a full densification of the fiber batches within 15 min soaking time only.

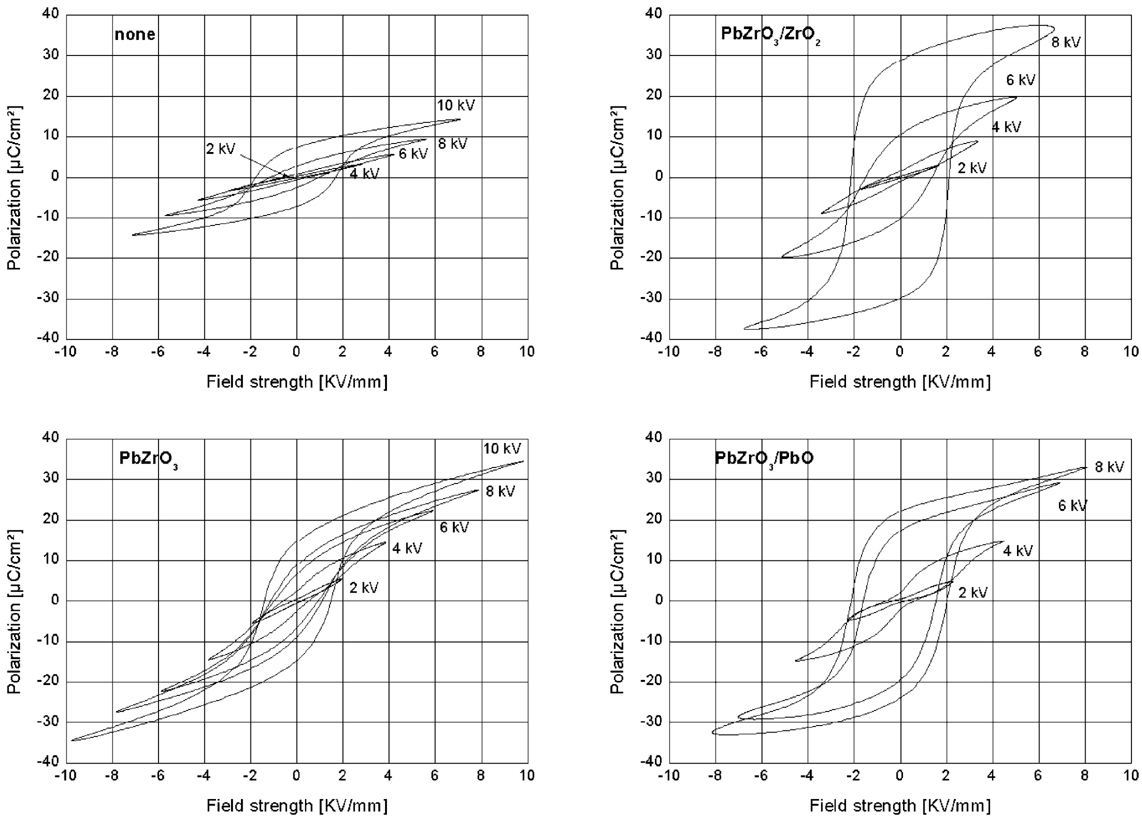


Fig. 15. Hysteresis loops of PZT fibers with a PbO excess of $z=+0.02$ in the spinning sol, sintered with various buffer systems; (a) none; (b) with $PbZrO_3/ZrO_2$; (c) PbZrO3; (d) $PbZrO_3/PbO$.

### 3.3.2. Di- and ferroelectric properties of PZT fibers sintered with different buffers

As expected, for all buffer systems increased $\epsilon_r$-values are obtained for fiber batches with $z=+0.14$ compared to fibers with $z=+0.02$, as shown in Table 3. This is due to the different residual porosity of the fibers: the $z=+0.14$ batches are devoid of residual porosity and therefore characterized by increased permittivities for all buffers.

The PZT fibers with $z=+0.14$ sintered devoid of a buffer system stand out as an exception. The strong data scattering is probably due to the large curvature of the fibers increasing their propensity to fracture during composite preparation. Because of the fractures the fiber permittivities calculated from those composites are no longer valid. Realistic and reproducible fiber permittivities can only be derived from batches sintered with $PbZrO_3$ buffer.

A comparison of the ferroelectric behaviour of identically prepared PZT fibers with a PbO content of $z=+0.02$ sintered with different buffers is given in Fig. 15. The shape of the hysteresis loops varies remarkably; best measurements were obtained for fibers sintered with $PbZrO_3/PbO$ buffer, but—as obtained from other measurements (not shown here)—those fibers show the strongest ageing-effects, too. Fibers sintered with $PbZrO_3/ZrO_2$ show hysteresis loops with high polarization values and a quite rectangular shape, too. Those hysteresis curves are devoid of constrictions due to ageing effects; together with the reasonable permittivity data this leads to the conclusion, that this combination of PbO content in the spinning sol and buffer system should be chosen for a further fiber optimization.

## 4. Conclusions

The sintering process of sol-gel derived PZT(53/47) fibers has been optimized via interaction of (1) varying the PbO level in the spinning sol, (2) different buffer systems for controlling the PbO partial pressure during sintering, and (3) variations of the soaking time. With this new approach full densification of the fiber microstructure can be achieved without sacrificing a 100% PZT yield.

Except for the highest excess PbO batch with $z=+0.14$ a buffer system is mandatory for PbO-deficient batches and batches with low PbO excess in order to achieve full densification. For $PbZrO_3/PbO$ buffers, the residual porosity is less than 1% for all PbO levels in the spinning sol studied. For PbO-rich buffer systems however, special care may be advised to prevent sticking-together of fibers, which results in curled fiber geometries and poorly reproducible functional properties. The sintering experiments confirm, that fine-tuning of the PbO partial pressure via buffer systems defines a necessary and highly effective tool complementary to the conventional approach of establishing a well-defined net PbO level in the spinning sol.

Sintering experiments with different holding times show, that at 900 °C a fully densified, homogeneous PZT microstructure with a narrow grain size distribution centered at approx. 1 μm is obtained within 15 min soaking time provided the PbO-level has been optimized for both the spinning sol and the buffer system.

All fiber batches sintered with a buffer consist of perowskite phase, devoid of crystalline secondary phases. A PbO-bearing non-crystalline phase was identified at triple grain junctions from PbO excess batches by small probe microanalysis in the TEM supporting that liquid-phase sintering is promoted in such systems. Densification of PbO-deficient batches is controlled by solid state sintering. A tensile strength level of 125 MPa was obtained for PZT fibers stabilized with a thin PVA coating. PZT fibers exhibit remanent polarization values of 14 $\mu C/cm^2$ with coercivities between 1.2 and 1.4 V/μm. The dielectric permittivities are in the range of 600–1000. Electromechanical strains in the order of 0.10% were obtained.

## Acknowledgements

This research has been supported by the Deutsche Forschungsgemeinschaft (DFG), SPP 734 through grants Br 923/4 and Mu 720/16. The stimulating discussions with the mentors of SPP 734, Professor Thomann and Professor Härdtl as well as B. Hildmann, DLR, are gratefully acknowledged. The authors appreciate the TEM preparation work performed by G. Paul, DLR.

## References

1. Uchino, K., Materials issues in design and performance of piezoelectric actuators: an overview. *Acta. Mater.*, 1998, **46**, 3745–3753.
2. Newnham, R. E., Molecular mechanisms in smart materials. *MRS Bulletin*, 1997, **5**, 20–34.
3. Newnham, R. E. and Ruschau, G. R., Smart electroceramics. *J. Am. Ceram. Soc.*, 1991, **74**(3), 463–480.
4. Haertling, G. H., Ferroelectric ceramics: history and technology. *J. Am. Ceram. Soc.*, 1999, **82**(4), 797–818.
5. Safari, A., Janas, V. F. and Bandyopadhyay, A., Development of fine-scale piezoelectric composites for transducers. *Ceramics Processing*, 1997, **43**(11A), 2849–2856.
6. Park, Y. I. and Miyayama, M., Electrical properties of $Pb(Zr_{0.53}Ti_{0.47})O_3$ [PZT] fibers fabricated by sol-gel technique. *Key Enginiering Materials*, 1999, **157–158**, 33–40.
7. Scholz, H., Watzka, W., Sporn, D., Seffner, L. and Schönecker, A., Processing and Properties of PZT-Fibers for 1–3 Composites. Proceedings of ICCM-10, Whistler, B.C., Canada, 1995, IV-481-IV-488.
8. Janas, V. F. and Safari, A., Overview of fine-scale piezoelectric ceramic/polymer composite processing. *J. Am. Ceram. Soc.*, 1995, **78**(11), 2945–2955.
9. James, A. D. and Messer, P. F., The preparation of transparent PLZT ceramics from oxide powders by liquid-phase sintering. *J. Br. Ceram. Soc.*, 1978, **77**, 152–158.
10. Kingon, A. and Clark, B., Sintering of PZT ceramics: I, atmosphere control. *J. Am. Ceram. Soc.*, 1983, **66**(4), 253–256.
11. Kingon, A. and Clark, B., Sintering of PZT ceramics: II, effect of PbO content on densification kinetics. *J. Am. Ceram. Soc.*, 1983, **66**(4), 256–260.
12. Snow, G. S., Fabrication of transparent electrooptic PLZT ceramics by atmosphere sintering. *J. Am. Ceram. Soc.*, 1973, **56**(2), 91–96.
13. Klicker, K. A., Biggers, J. V. and Newnham, R. E., Composites of PZT and epoxy for hydrostatic transducer applications. *J. Am. Ceram. Soc.*, 1981, **64**(1), 5–9.
14. Savakus, H. P., Klicker, K. A. and Newnham, R. E., PZT-epoxy piezoelectric transducers: a simplified fabrication procedure. *Mater. Res. Bull.*, 1981, **16**, 677–680.
15. Lubitz, R. E., Wolff, A., Preu, G. and Schulmeyer, B., New piezoelectric composites for ultrasonic transducers. *Ferroelectrics*, 1993, **133**(1–4), 21–26.
16. Gentilman, R.L., Fiore, D.F., Pham, H.T., French, K.W. and Bowen, L.J., Fabrication and properties of 1-3 PZT-polymer composites. Bhalla, A.S., Nair, K.M., Lloyd, I.K., Yanagida, H. and Payne, D.A. (eds.) In *Ferroic Materials: Design, Preparation and Characteristics, Amer. Cer. Soc.*, 43, 1994, p. 239.
17. Steinhausen, R., Hauke, T., Seifert, W., Beige, H., Watzka, W., Seifert, S., Sporn, D., Starke, S. and Schönecker, A., Finescaled piezoelectric 1-3 composites: properties and modelling. *J. Eur. Ceram. Soc.*, 1999, **19**, 1289–1293.
18. Hansch, R., Seifert, S., Braue, W., Sporn, D. and Müller, G., (in preparation).
19. Helke, G., Seifert, S. and Cho, S.-J., Phenomenological and structural properties of piezoelectric ceramics based on $xPb(Zr,Ti)O_3$-$(1\text{-}x)Sr(K_{0.25}Nb_{0.75})O_3$ (PZT/SKN) solid solutions. *J. Eur. Ceram. Soc.*, 1999, **19**, 1265–1268.
20. Glaubitt, W., Watzka, W., Scholz, H. and Sporn, D., Sol-gel processing of functional and structural ceramic oxide fibers. *J. Sol-Gel Sci. and Technology*, 1997, **8**, 29–33.
21. Williams, D. B. and Carter, C. B., *Transmission Electron Microscopy, A Textbook for Materials Science*. Plenum Press, New York, 1996.
22. European Prestandard DIN V ENV 1007 part 4, May 1994, Determination of tensile properties of ceramic filament at ambient temperature. Beuth Verlag GmbH, Berlin, 1994.
23. Sorge, G., Hauke, T. and Klee, M., Electromechnical properties of thin ferroelectric $Pb(Zr_{0.53}Ti_{0.47})O_3$-layers. *Ferroelectrics*, 1995, **163**(1–4), 77–88.
24. Akbas, M., Michael, A., McCoy, A. and Lee, W. E., Microstructural evolution during pressureless sintering of PbO lanthanum zirconate titanate ceramics with excess PbO(II) oxide. *J. Am. Ceram. Soc.*, 1995, **78**(9), 2417–2424.
25. Hammer, M. and Hoffmann, M. J., Sintering model for mixed-oxide-derived PbO zirconate titanate ceramics. *J. Am. Ceram. Soc.*, 1998, **81**(12), 3277–3284.
26. Atkin, R. B. and Fulrath, R. M., Point defects and sintering of PbO zirconate-titanate. *J. Am. Ceram. Soc.*, 1971, **54**(5), 265–270.
27. Helke, G., private communication.
28. Jaffe, H., Cook, W. R. and Jaffe, H., *Piezoelectric Ceramics*. Academic Press, London, 1971.
29. Xu, Y., *Ferroelectric Materials and their Applications*. Elsevier Sci. Pub., Amsterdam, 1991.